ornl

OAK RIDGE NATIONAL LABORATORY

LOCKHEED MARTIN

MANAGED AND OPERATED BY
LOCKHEED MARTIN ENERGY RESEARCH CORPORATION
FOR THE UNITED STATES
DEPARTMENT OF ENERGY

ORNL-27 (3-96)

ORNL/NRC/LTR-99/6

Investigation of the Impact of ENDF/B-VI Cross Sections on the H. B. Robinson-2 Pressure-Vessel Flux Prediction

I. Remec

ORNL/NRC/LTR-99/6

Contract Program or Title:	**Embrittlement Data Base and Dosimetry Evaluation Program**
Subject of this Document:	**Investigation of the Impact of ENDF/B-VI Cross Sections on the H. B. Robinson-2 Pressure-Vessel Flux Prediction**
Type of Document:	**Letter Report**
Author:	**I. Remec**
Date of Document:	**June 1999**
Responsible NRC Individual and NRC Office or Division:	**C. Fairbanks (301-415-6014) Division of Engineering, U.S. Nuclear Regulatory Commission**

Prepared for the
U.S. Nuclear Regulatory Commission
Washington, DC 20555
under Interagency Agreement DOE 1886-N616-4W
NRC JCN No. W6164

OAK RIDGE NATIONAL LABORATORY
Oak Ridge, TN 37831-6363
managed by
LOCKHEED MARTIN ENERGY RESEARCH CORP.
for the
U.S. Department of Energy
under contract DE-AC05-96OR22464.

ORNL/NRC/LTR-99/6

Investigation of the Impact of ENDF/B-VI Cross Sections on the H. B. Robinson-2 Pressure-Vessel Flux Prediction

I. Remec

Manuscript Completed - May 1999
Date Published - June 1999

Prepared for the
U.S. Nuclear Regulatory Commission
Washington, DC 20555
under Interagency Agreement DOE 1886-N616-4W

NRC JCN No. W6164

Prepared by the
OAK RIDGE NATIONAL LABORATORY
Oak Ridge, TN 37831-6363
managed by
LOCKHEED MARTIN ENERGY RESEARCH CORP.
for the
U.S. Department of Energy
under contract DE-AC05-96OR22464

DISCLAIMER

DISCLAIMER

Portions of this document may be illegible in electronic image products. Images are produced from the best available original document.

ABSTRACT

This report discusses the impact of the change from the SAILOR cross-section library, based on the ENDF/B-IV data, to the BUGLE-96 cross-section library, based on the ENDF/B-VI data, on the neutron flux prediction in the H. B. Robinson-2 pressure vessel, in the surveillance capsule, and in the cavity.

The fast flux (E > 1 MeV) from the transport calculations with the BUGLE-96 library is ~6% higher in the surveillance capsule and at the PV inner wall, and ~25% higher in the reactor cavity than the flux from the transport calculations with the SAILOR library. These changes result from the combined effect of the changes in the cross sections, which cause significant increases in the calculated fluxes, and much smaller decreases in the fast fluxes due to the changes in the fission spectra. The increase in the calculated fast flux due to the changes in the cross sections only is ~9% in the capsule and at the pressure vessel (PV) wall, and ~30% in the cavity. The changes in the fission spectra lead to decreases in the order of ~3–4% in calculated fast fluxes.

The neutron flux, used to evaluate the surveillance capsules and to assess the PV embrittlement, is often determined by techniques that combine measurements and calculations, such as scaling or spectrum adjustment. Only the simplest method—the scaling—was investigated in this report. When the measured reaction rates were used to scale the calculated fluxes, the differences between the BUGLE-96 and SAILOR scaled fluxes were 9% in the capsule and at the PV inner wall, and 15% in the cavity, with the BUGLE-96 values being higher. The scaling effectively reduced the differences between the fluxes in the cavity from 30% to 15%; however, it unexpectedly increased the differences in fluxes in the capsule from ~6% to 9%. The calculation with the SAILOR cross-section library and ENDF/B-VI fission spectra resulted in the lowest calculated fast-flux values at all locations considered. However, when scaled with measured reaction rates the scaled fluxes agreed within 2% with the BUGLE-96 scaled fluxes. This agreement illustrates that while the changes in fission spectra have only a minor impact on the calculated fast fluxes, they are important for the comparison of the calculated and the measured reaction rates and, consequently, for the fast flux determined by any technique that combines the calculations and the measurements. The transport calculations with the ENDF/B-VI fission spectra, compared with the calculations with the ENDF/B-IV fission spectra, show improved consistency of the C/M ratios for the dosimeters sensitive to different energy ranges, hence indicating that the calculated spectrum is in better agreement with the actual neutron spectrum during the irradiation.

The changes in the fast-flux values from the transport calculations, due to the change from the SAILOR to the BUGLE-96 library, which are reported in this paper, should be representative for the PWRs similar to the HBR-2. When calculations are combined with measurements to produce the fast-flux estimates, the changes in the fast flux due to the change of the cross-section library should in general be smaller that the changes in the fluxes from the transport calculation alone. However, the actual changes will be case-specific and will depend on the particular technique used to combine the calculations and measurements.

CONTENTS

TABLES

FIGURES

ACKNOWLEDGMENTS

The author wishes to express his appreciation to the reviewers, J. V. Pace III and R. E. Stoller of the Oak Ridge National Laboratory. Special thanks go to C. H. Shappert for providing the editorial review and to M. R. Whittenbarger for the preparation of this report. The work was performed as a part of the "Embrittlement Data Base and Dosimetry Evaluation Program" (FIN W6164) sponsored by the Nuclear Regulatory Commission and managed by Carolyn Fairbanks of the Nuclear Regulatory Commission.

1. INTRODUCTION

Version VI of the U.S. Evaluated Nuclear Data File (ENDF/B-VI) was released in 1990 (Ref. 1). Seventy-four of the 320 cross-section evaluations contained in the library were new for Version 6. Following the initial release of ENDF/B-VI, revisions and some new evaluations were prepared and released. Among the new evaluations in the ENDF/B-VI, which are of greatest interest to the reactor pressure vessel (PV) surveillance community, are the evaluations of the iron cross sections. These evaluations introduced cross sections for individual iron isotopes, reduced inelastic scattering cross sections, and increased the forward-directed angular distributions of inelastically scattered neutrons. These changes were expected to reduce the under predictions of neutron transmission through thick layers of iron, which had been typical for the neutron transport calculations with pre-ENDF/B-VI cross sections. Several format changes were also introduced in ENDF/B-VI. These changes were thoroughly prepared; however, they necessitated changes in processing codes and resulted in considerable delay between the release of ENDF/B-VI and the completion of the multigroup cross-section libraries based on ENDF/B-VI data. The first broad-group library based on ENDF/B-VI and released for general distribution was BUGLE-93 (Ref. 2), released in February 1993. Subsequent work led to the preparation of BUGLE-96 (based on ENDF/B-VI, Release 3, distributed in May 1995, [Ref. 3]). BUGLE-96 is expected to replace the SAILOR (Ref. 4) and BUGLE-80 (Ref. 5) libraries for routine PV flux calculations. Therefore, it is of interest to assess the impact of the new cross-section library on the calculated PV flux and on the evaluation of PV surveillance dosimeters. This work presents the transport calculations of the PV multigroup neutron fluxes with SAILOR and BUGLE-96 libraries. The calculated dosimeter reaction rates are compared with the measured ones for the location of the in-vessel surveillance capsule dosimeters and for the dosimeters located outside the PV in the reactor cavity. The calculations are performed for the H. B. Robinson-2 (HBR-2) power plant, which is a 2300-MW (thermal) pressurized light-water reactor designed by Westinghouse. All HBR-2 plant data used in the analysis, including the power distribution and the measured specific activities, were taken from Reference 6.

2. ANALYSIS

The transport calculations were performed using the DORT computer code (Ref. 7) and the flux synthesis method.* The flux synthesis method, described in more detail in Reference 8, uses one- and two-dimensional (1-D and 2-D) transport calculations to obtain an estimation of the neutron fluxes in the three-dimensional (3-D) geometries. All transport calculations were performed as fixed neutron source calculations. The P_3 expansion of the angular dependence of the scattering cross sections, and a symmetric S_8 "directional quadrature set" (i.e., a set of discrete directions and angular quadratures) were used for all transport calculations. The details of the modeling are described in Reference 6 and will not be repeated here. Exactly the same calculational procedure, models, and code numerical parameters were used for all the calculations. The only input data varied were the cross sections for the transport and the fission spectrum of the neutron source. This procedure guarantees that all the differences observed are due to the changes in cross sections and

*DORT version 3.2, dated October 1, 1997, was used.

the fission spectrum. The cross sections for the transport calculations were prepared with the GIP code (Ref. 9) and were taken from the SAILOR and BUGLE-96 libraries.

3. RESULTS AND DISCUSSION

Reaction rates for the dosimeters in the surveillance capsule located in the downcomer region inside the PV and at the cavity location were calculated. The comparison of reaction rates obtained with multigroup neutron fluxes calculated with the BUGLE-96 and SAILOR cross-section libraries is presented in Table 1. In the calculation with SAILOR, the same spectrum of the fixed neutron source was used as in the calculation with the BUGLE-96 library, which used the fission spectrum half-way between the ^{235}U and ^{239}Pu thermal neutron fission spectrum.** Therefore, all the differences in Table 1 are due to the change of cross sections for transport calculation from SAILOR (ENDF/B-IV) to BUGLE-96 (ENDF/B-VI). In the surveillance capsule location, BUGLE-96 resulted in ~8% higher reaction rates, while at the cavity location, the BUGLE-96 reaction rates were ~29% higher. The reaction rate ratios for different dosimeters, sensitive to different energy ranges, are quite consistent, which is reflected in the small standard deviations of the average reaction rate ratios of 3% in the capsule and 5% in the cavity. The only deviation from the average behavior observed is for the ^{63}Cu(n, α) reaction, which experiences a smaller increase than the other reactions due to the change from SAILOR to BUGLE-96. The ^{63}Cu(n, α) reaction has the highest threshold, and ~90% of the ^{63}Cu(n, α) reactions are due to the neutrons with energies above 6 MeV.

A comparison of the calculated and measured reaction rates for the calculations with the SAILOR and BUGLE-96 libraries is given in Table 2. The average calculated-to-measured (C/M) ratio in the capsule is 0.84 and 0.91 for the SAILOR and BUGLE-96, respectively, and the standard deviation of the average is 0.04 for both libraries. In the cavity the average C/M is 0.72 and 0.92 for the SAILOR and for the BUGLE-96 libraries, respectively, and the standard deviation of the average is 0.06 for both libraries. The calculation with the BUGLE-96 library greatly improves the agreement of the calculations with the measurements and circumvents the decrease of C/M ratios with increasing thickness of steel penetrated, which is quite pronounced in the SAILOR results. The average C/M values in the cavity are calculated without the ^{237}Np dosimeter, because there are unresolved concerns about the reliability of the ^{237}Np measurement (see, for example, Reference 10).

The comparison of the calculated fast fluxes is given in Table 3. The fast flux (E > 1 MeV) calculated with the BUGLE-96 library is 9% higher than the SAILOR fast flux in the capsule and at the PV inner radius, 13 % higher in the PV, at one-quarter of the PV wall thickness from the inner surface of the vessel, and 31% higher at the location of the dosimeters in the reactor cavity.

The effect of the change of the cross sections for transport calculations from the SAILOR (ENDF/B-IV) to the BUGLE-96 (ENDF/B-VI) are the following: (1) ~9% increase in the fast

---

**The fix-source energy spectrum input into the transport calculations was calculated as 0.5* χ(U-235) + 0.5* χ(Pu-239). The U-235 and Pu-239 thermal neutron fission spectra were taken from BUGLE-96.

neutron flux and the threshold reaction rates of the typical surveillance dosimeters at the location of the in-vessel capsule, and (2) ~30% increase in the fast flux and reaction rates in the cavity.

Before the ENDF/B-VI cross-section libraries became available, the transport calculations with the SAILOR library were performed with the fission spectra from the ENDF/B-IV for the energy spectrum of the fixed source. Therefore, in this study the calculations with the SAILOR library were done also with the source fission spectrum from ENDF/B-IV. Again the average of the ^{235}U and ^{239}Pu fission spectra was used; however, the ^{235}U fission spectrum was taken from the SAILOR library and the ^{239}Pu fission spectrum (which is not given in the SAILOR library) was taken from VITAMIN-C library (Ref. 11) and collapsed into the 47 energy groups used in SAILOR. The VITAMIN-C library is the fine-group library based on ENDF/B-IV data from which the SAILOR library was generated.

The results from the calculation that used SAILOR and the ENDF/B-IV fission spectrum are compared with results from the BUGLE-96 calculations in Tables 4–6. The comparison of the calculated reaction rates, given in Table 4, shows that the BUGLE-96 calculations give slightly higher reaction rates for most of the reactions at the capsule location. However, there is a significant variation of the reaction-rate ratios with the reaction threshold, which is not present in Table 1. For the lowest threshold reaction (i.e., $^{237}Np(n,f)$) BUGLE-96 gives 6% higher reaction rates than SAILOR with the ENDF/B-IV fission spectrum. With increasing threshold (the reaction threshold increases from the left to the right in Table 4), the ratio of reaction rates decreases and for $^{46}Ti(n,p)$ and $^{63}Cu(n,\alpha)$, the SAILOR calculation gives higher reaction rates. For the $^{63}Cu(n,\alpha)$ reaction the BUGLE-96 calculation gives an approximately 18% lower reaction rate. Due largely to the $^{63}Cu(n,\alpha)$ reaction, the average BUGLE-to-SAILOR reaction-rate ratio in the capsule is 0.98. The standard deviation of the average is 0.09, which reflects the considerable scatter of the reaction rate ratios, and is much higher than the corresponding value in Table 1, which is 0.03. In the cavity the situation is similar to the one in the capsule, only that the trend is more pronounced. For the $^{237}Np(n,f)$ reaction and the $^{63}Cu(n,\alpha)$ reaction, BUGLE-96 gives 25% higher and 10% lower reaction rates, respectively, than SAILOR with the ENDF/B-IV fission spectrum. On the average the BUGLE-96 calculation predicts 13% higher reaction rates in the cavity than the SAILOR calculation, and the standard deviation of the average ratio is ~12%, again reflecting the considerable variation of reaction-rate ratios with increasing thresholds of the reactions.

A comparison of the calculated and measured reaction rates, obtained with the SAILOR library and the ENDF/B-IV fission spectra, is given in Table 5. The average C/M ratios are 0.94 in the capsule and 0.84 in the cavity, while the values obtained with the SAILOR and ENDF/B-VI fission spectra were 0.84 and 0.72, respectively. The use of the ENDF/B-IV fission spectrum with SAILOR gives better C/M ratios; however, it also introduces the considerable systematic variation of C/M ratios with reactions threshold. Larger variations of the C/M ratios are reflected in larger standard deviations of the average C/M ratios, which are 0.10 in the capsule and 0.14 in the cavity, but the corresponding values in Table 2 are 0.04 and 0.06, respectively.

A comparison of the fast fluxes is presented in Table 6. The two calculations with the SAILOR library—the one with the ENDF/B-IV and the one with the ENDF/B-VI fission spectra—give only slightly different fast fluxes. The differences are ~3–4% and the calculation with ENDF/B-VI fission spectra gives lower values. These differences are much smaller than the shift in the average C/M

ratios, which change from 0.94 to 0.84 in the capsule and from 0.84 to 0.72 in the cavity (see Table 5) when the ENDF/B-IV fission spectrum is replaced with the ENDF/B-VI fission spectrum in the calculation with the SAILOR library. The reason for this is that the greatest changes in spectrum occur at the high-energy end (above 4 MeV), which does not contribute significantly to the flux above 1 MeV because of the sharp decrease in the spectrum with increasing energy. However, the neutrons in this energy range create practically all of the ^{46}Ti(n,p) and ^{63}Cu(n,α) reactions and, consequently, the calculated reactions rates of these dosimeters are strongly affected by the changes in the spectrum in this energy range. The fast neutron flux calculated with the BUGLE-96 library is higher than the flux obtained from the calculation with SAILOR with the ENDF/B-IV fission spectrum by 6% in the capsule and at the PV inner wall, by 10% at one-quarter of the PV wall thickness from the PV inner wall, and by 25% at the location of the dosimeters in the cavity.

Detailed comparisons of the calculated multigroup neutron fluxes are presented in Figures 1–3. A comparison of the spectra in the capsule and in the cavity, calculated with the BUGLE-96 and SAILOR libraries and with the ENDF/B-VI fission spectrum, is shown in Figure 1. BUGLE-96 gives higher neutron fluxes at all energies except for a few energy groups. The particularly important increases in group fluxes are observed above ~0.1 MeV. Figure 2 gives a similar comparison as in Figure 1, except that the SAILOR calculation used the ENDF/B-IV fission spectrum. Again, BUGLE-96 gives higher group fluxes over most of the energy range, except above ~4 MeV, where the SAILOR fluxes are higher. Even though the curves shown in Figures 1 and 2 are similar below ~4 MeV, the change in the shape above 4 MeV is quite pronounced. This is further illustrated in Figure 3, where the multigroup fluxes from the two SAILOR calculations are compared. The calculation with the ENDF/B-IV fission spectrum gives drastically higher fluxes above ~4 MeV than the calculation with the ENDF/B-VI fission spectrum. These differences can, of course, be traced to the differences in the ENDF/B-IV and the ENDF/B-VI fission spectra. The spectra of thermal-neutron-induced fissions of ^{235}U, ^{239}Pu, and the average of the ^{235}U and the ^{239}Pu spectra are compared in Figure 4. Clearly, there are much fewer neutrons in the BUGLE-96 fission spectra above ~4MeV than in the SAILOR (and VITAMIN-C) spectra.

In most cases the determination of the PV neutron flux involves not only the calculations but also the measurements. The measured reaction rates of the dosimeters can be combined with the calculated multigroup fluxes in different ways (e.g., by neutron spectrum adjustment technique) to produce the best estimates of the neutron flux at the location of metallurgical specimens in the capsule and inside the PV wall. The simplest, yet often-used technique, is to scale the calculated fast neutron flux with the measured reaction rates. This technique can be accomplished, for example, by dividing the calculated fast flux with the average C/M reaction-rate ratio. Even though this simplistic approach has its obvious shortcomings (see, for example, Reference 12), it will be used here to further assess the impact of the change from ENDF/B-IV to ENDF/B-VI cross sections and fission spectra. The scaled fast fluxes, listed in Table 7, at the capsule and the cavity locations were obtained by dividing the fast fluxes from transport calculations (given in parentheses) by the average C/M values (from Table 5) at the capsule and cavity locations, respectively. The scaled flux at the PV inner radius was obtained by dividing the scaled flux value in the capsule by the lead factor (given in the last row in Table 7). The lead factor is the ratio of the calculated fast flux in the capsule and the fast flux at the PV inner radius, at the location where the fast flux on the PV wall reaches its maximal value; therefore, the same scale factor is used for the capsule and the PV inner-wall

location. At the location of the cavity dosimeters the scaled fast flux was determined by dividing the calculated flux with the average C/M value for the location of the cavity dosimeters.

Several observations can be made regarding the results in Table 7. The three calculations, namely, the BUGLE-96, SAILOR with ENDF/B-VI fission spectrum, and SAILOR with the ENDF/B-IV fission spectrum, predicted practically identical lead factors. This agreement indicates that all three calculations predicted the same fast-flux attenuation from the capsule to the PV wall. The scaling effectively removed the differences between the fast fluxes calculated with the BUGLE-96 library and the fast fluxes calculated with the SAILOR library with the ENDF/B-VI fission spectrum. The differences in scaled fast fluxes are only about 1–2%, while the differences in the calculated fluxes were 9% in the capsule and at the PV wall, and 31% in the cavity.

For the calculation with the SAILOR and ENDF/B-IV fission spectrum, the scaling reduced the differences to the BUGLE-96 results in the cavity from 25% to 15%. At the capsule and at the PV inner wall the differences between the scaled fluxes are 9% and are higher than the differences between the calculated fluxes, which are 6%. This surprising result, namely, that the scaled fluxes differ more than the fluxes from the transport calculation, clearly demonstrates one of the shortcomings of the scaling. The scaling does not take into account that the dosimeters are sensitive to different ranges of neutron energies, and, consequently, each dosimeter should be used to adjust the neutron spectrum only in the energy range to which it is sensitive. In the case when there is a considerable variation of the C/M values for different dosimeters, the scaling may be hard to justify. This situation is especially true if the trend is systematic, as was observed for the SAILOR calculation with the ENDF/B-IV fission spectrum, where the C/M values showed systematic increasing with increasing reaction threshold energy. The high C/M values for the two reactions with the highest thresholds (i.e., ^{46}Ti(n,p) and ^{63}Cu(n,α)), which are sensitive only to the small fraction of neutrons with energies above 1 MeV, keep the average C/M value for the calculation with the SAILOR and ENDF/B-IV fission spectrum relatively high (see Table 5). Consequently, the scaling produces smaller increases of the fast fluxes. The result is, that, while the calculation with SAILOR and the ENDF/B-VI fission spectrum gave the lowest fast-flux values at all locations considered, the lowest values of the scaled fast fluxes were those obtained from the SAILOR and ENDF/B-IV fission spectrum.

Despite the shortcomings described above, the dosimetry measurements in most cases helped to substantially reduce the differences in fast fluxes obtained from different calculations. The use of more elaborate methods for combining the calculations and the measurements, such as the spectrum adjustment technique, should produce better results and should circumvent the difficulties related to the scaling method.

4. CONCLUSIONS

The change from the SAILOR library, based on the ENDF/B-IV data, to the BUGLE-96 library, based on the ENDF/B-VI data has the following impact on the H. B. Robinson-2 PV flux prediction.

The calculated fast flux, obtained with the BUGLE-96 library is ~6 % higher in the surveillance capsule and at the PV inner wall, and ~25% higher in the reactor cavity. These changes result from the combined effect of the changes in the cross sections, which cause significant increases in the calculated fluxes, and much smaller decreases in the fast fluxes due to the changes in the fission spectra. The increase in the calculated fast flux due to changes in the cross sections only is ~9% in the capsule and at the PV wall, and ~30% in the cavity. The changes in the fission spectra only lead to minor decreases of the order of 3–4% in calculated fast fluxes.

Even though the changes in the fission spectra do not have a significant impact on the calculated fast fluxes, they are important for the comparison of calculated and measured reaction rates and consequently for fast-flux determination by techniques that combine measurements and calculations, such as scaling or spectrum adjustment. The transport calculations with the ENDF/B-VI fission spectra, compared with the calculations with ENDF/B-IV fission spectra, show improved consistency of the C/M ratios for the dosimeters sensitive to different energy ranges, hence indicating that the calculated spectrum is in better agreement with the actual neutron spectrum during the irradiation.

When the measured reaction rates were used to scale the calculated fluxes, the differences between the BUGLE-96 and SAILOR scaled fluxes were 9% in the capsule and at the PV inner wall, and 15% in the cavity, with BUGLE-96 values being higher.

The calculation with the SAILOR cross-section library and ENDF/B-VI fission spectra resulted in the lowest calculated fast-flux values at all locations considered. However, when scaled with measured reaction rates the scaled fluxes agreed within 1–2% with the BUGLE-96 scaled fluxes.

The changes in the fast-flux values, obtained from the transport calculations, due to the change from the SAILOR to the BUGLE-96 library should be representative for reactors similar to HBR-2. When calculations are combined with the measurements to produce the fast-flux estimates, the changes in fast flux due to the change of the cross-section library should, in general, be smaller than the changes in the calculated values alone. However, the actual changes will be case-specific and will depend on the particular technique used to combine the calculations and measurements.

5. REFERENCES

1. P. F. Rose, "ENDF/B-VI Summary Documentation," BNL-NCS-17541 (ENDF-201) 4th Ed. (October 1991).

2. D. T. Ingersoll et al.,"Bugle-93: Coupled 47 Neutron, 20 Gamma-Ray Group Cross-Section Library Derived from ENDF/B-VI for LWR Shielding and Pressure Vessel Dosimetry Applications," RSICC Data Library Collection, DLC-175, Oak Ridge National Laboratory, February 1994.

3. J. E. White et al.,"BUGLE-96: Coupled 47 Neutron, 20 Gamma-Ray Group Cross Section Library Derived from ENDF/B-VI for LWR Shielding and Pressure Vessel Dosimetry Applications," RSICC Data Library Collection, DLC-185, Oak Ridge National Laboratory, March 1996.

4. G. L. Simmons et al., "Analysis of the Browns Ferry Unit 3 Irradiation Experiments," EPRI NP-3719 (November 1984), RSICC Data Library Collection, DLC-076/SAILOR; (Sailor, Coupled Self-Shielded, 47-Neutron, 20-Gamma-Ray, P_3, Cross Section Library for Light Water Reactors).

5. R. W. Roussin, "BUGLE-80: Coupled 47 Neutron, 20 Gamma-Ray, P3, Cross-Section Library for LWR Shielding Calculations," Informal Notes, Radiation Shielding Information Center (RSICC) Data Library Collection, DLC-075/BUGLE-80, Oak Ridge National Laboratory, 1980.

6. I. Remec and F. B. K. Kam, "H. B. Robinson-2 Pressure Vessel Benchmark," NUREG/CR-6453, ORNL/TM-13240, Oak Ridge National Laboratory, 1998.

7. W. A. Rhoades et al., "TORT-DORT Two- and Three-Dimensional Discrete Ordinates Transport, Version 2.8.14," CCC-543, Radiation Shielding Information Center, Oak Ridge National Laboratory, 1994.

8. R. E. Maerker, "LEPRICON Analysis of the Pressure Vessel Surveillance Dosimetry Inserted into H. B. Robinson-2 During Cycle 9," *Nuc. Sci. Eng.*, 96:263 (1987).

9. W. A. Rhoades, "The GIP Program for Preparation of Group-Organized Cross-Section Libraries," informal notes, RSICC Peripheral Shielding Routine Collection PSR-75, Oak Ridge National Laboratory, 1975.

10. I. Remec, *Analysis of the Discrepancy in the ^{237}Np Dosimeter for the H. B. Robinson Unit 2 Cavity Benchmark Experiment, Cycle 9: Initial Phase*, ORNL/NRC/LTR-97/6, Oak Ridge National Laboratory, 1997.

11. R. W. Roussin et al., "VITAMIN-C: The CTR Processed Multigroup Cross-Section Library for Neutronics Studies," ORNL/RSIC-37, RSICC Data Library Collection DLC-41/VITAMIN-C, Oak Ridge National Laboratory, 1980.

12. F. B. K. Kam et al., *Pressure Vessel Fluence Analysis and Neutron Dosimetry*, NUREG/CR-5049, ORNL/TM-10651, Oak Ridge National Laboratory, 1987.

Table 1 Ratios of the reaction rates calculated with BUGLE-96 (ENDF/B-VI) and SAILOR (ENDF/B-IV). BUGLE-96 fission spectra were used in both calculations

	^{237}Np (*n,f*) ^{137}Cs	^{238}U (*n,f*) ^{137}Cs	^{58}Ni (*n,p*) ^{58}Co	^{54}Fe (*n,p*) ^{54}Mn	^{46}Ti (*n,p*) ^{46}Sc	^{63}Cu (*n,α*) ^{60}Co	Average ± σ
Capsule							
BUGLE-96/ SAILOR	1.08	1.09	1.11	1.11	1.08	1.03	1.08 ± 0.03
Cavity							
BUGLE-96/ SAILOR	1.29	1.31	1.33	1.34	1.28	1.19	1.29 ± 0.05

Table 2 The calculated-to-measured (C/M) reaction rate ratios for the BUGLE-96 and SAILOR libraries. BUGLE-96 fission spectra were used in both calculations

	^{237}Np (*n,f*) ^{137}Cs	^{238}U (*n,f*) ^{137}Cs	^{58}Ni (*n,p*) ^{58}Co	^{54}Fe (*n,p*) ^{54}Mn	^{46}Ti (*n,p*) ^{46}Sc	^{63}Cu (*n,α*) ^{60}Co	Ave. C/M ± σ
Capsule							
BUGLE-96	0.92	0.89	0.96	0.93	0.85	0.93	0.91 ± 0.04
SAILOR	0.85	0.82	0.86	0.84	0.78	0.90	0.84 ± 0.04
Cavity							
BUGLE-96	0.61	0.82	0.97	0.96	0.90	0.96	0.92 ± 0.06* (0.87 ± 0.14)
SAILOR	0.48	0.63	0.73	0.71	0.71	0.80	0.72 ± 0.06* (0.68 ± 0.11)

* The average C/M ratios *without* the C/M for the Np-237 dosimeter. (Values in parentheses are obtained *with* the C/M for the Np-237 dosimeter)

Table 3 Comparison of fast fluxes (E > 1 MeV) calculated with SAILOR and BUGLE-96 libraries. BUGLE-96 fission spectra were used in both calculations

	$\phi_{E>1MeV}$ ($cm^{-2}s^{-1}$)		
	SAILOR	BUGLE-96	BUGLE-96/ SAILOR
Capsule	3.825 E+10	4.175 E+10	1.09
PV inner radius	2.792 E+10	3.042 E+10	1.09
1/4 T PV	1.425 E+10	1.611 E+10	1.13
Cavity	5.969 E+8	7.793 E+8	1.31

Table 4 Ratios of the reaction rates calculated with BUGLE-96 (ENDF/B-VI) and SAILOR (ENDF/B-IV). In the calculation with SAILOR, the ENDF/B-IV fission spectra were used

	^{237}Np (n,f) ^{137}Cs	^{238}U (n,f) ^{137}Cs	^{58}Ni (n,p) ^{58}Co	^{54}Fe (n,p) ^{54}Mn	^{46}Ti (n,p) ^{46}Sc	^{63}Cu (n,α) ^{60}Co	Average ± σ
Capsule							
BUGLE-96/ SAILOR	1.06	1.04	1.02	1.01	0.92	0.82	0.98 ± 0.09
Cavity							
BUGLE-96/ SAILOR	1.25	1.23	1.19	1.19	1.04	0.90	1.13 ± 0.14

Table 5 The C/M ratios for the BUGLE-96 and SAILOR libraries

	^{237}Np (n,f) ^{137}Cs	^{238}U (n,f) ^{137}Cs	^{58}Ni (n,p) ^{58}Co	^{54}Fe (n,p) ^{54}Mn	^{46}Ti (n,p) ^{46}Sc	^{63}Cu (n,α) ^{60}Co	Ave. C/M ± σ
Capsule							
BUGLE-96	0.92	0.89	0.96	0.93	0.85	0.93	0.91 ± 0.04
SAILOR and ENDF/B-VI fission spectra	0.85	0.82	0.86	0.84	0.78	0.90	0.84 ± 0.04
SAILOR and ENDF/B-IV fission spectra	0.88	0.86	0.94	0.92	0.93	1.13	0.94 ± 0.10
Cavity							
BUGLE-96	0.61	0.82	0.97	0.96	0.90	0.96	0.92 ± 0.06* (0.87 ± 0.14)
SAILOR and ENDF/B-VI fission spectra	0.48	0.63	0.73	0.71	0.71	0.80	0.72 ± 0.06* (0.68 ± 0.11)
SAILOR and ENDF/B-IV fission spectra	0.49	0.67	0.81	0.80	0.87	1.06	0.84 ± 0.14* (0.78 ± 0.19)

* The average C/M ratios *without* the C/M for the Np-237 dosimeter. (Values in parentheses are obtained *with* the C/M for the Np-237 dosimeter)

Table 6 Comparison of the fast fluxes (E > 1 MeV) calculated with SAILOR and BUGLE-96 libraries.

	$\phi_{E>1MeV}$ ($cm^{-2}s^{-1}$)			Ratio	
	SAILOR + ENDF/B-IV Fiss. Spec.	SAILOR + ENDF/B-VI Fiss. Spec	BUGLE-96	(SAILOR + ENDF/B-VI Fiss. Spec.)/ (SAILOR + ENDF/B-IV Fiss. Spec.)	BUGLE-96/ (SAILOR + ENDF/B-IV Fiss. Spec.)
Capsule	3.943 E+10	3.852 E+10	4.175 E+10	0.97	1.06
PV inner radius	2.872 E+10	2.792 E+10	3.042 E+10	0.97	1.06
1/4 T PV	1.468 E+10	1.425 E+10	1.611 E+10	0.97	1.10
Cavity	6.214 E+8	5.969 E+8	7.793 E+8	0.96	1.25

Table 7 Comparison of scaled fast fluxes and lead factors (LF)

	$\phi_{E>1MeV}$ ($cm^{-2}s^{-1}$)			Ratios	
	SAILOR with ENDF/B-IV Fiss. Spec.	SAILOR with ENDF/B-VI Fiss. Spec.	BUGLE-96	BUGLE-96/ SAILOR with ENDF/B-IV Fiss. Spec.	BUGLE-96/ SAILOR with ENDF/B-VI Fiss. Spec.
Capsule	4.195 E+10 (3.943E+10)**	4.554 E+10 (3.825 E+10)	4.588 E+10 (4.175E+10)	1.09 (1.06)	1.01 (1.09)
PV inner radius	3.055 E+10 (2.872 E+10)	3.324 E+10 (2.792 E+10)	3.343 E+10 (3.042 E+10)	1.09 (1.06)	1.01 (1.09)
Cavity	7.398 E+8 (6.214 E+8)	8.290 E+8 (5.969 E+8)	8.471 E+8 (7.793 E+8)	1.15 (1.25)	1.02 (1.31)
LF*	1.373	1.370	1.372	1.00	1.00

* Lead factor (LF) is the ratio of the calculated fast flux at the capsule location to the maximum fast flux at the PV inner wall.

** Fast-flux values in parentheses are from transport calculations.

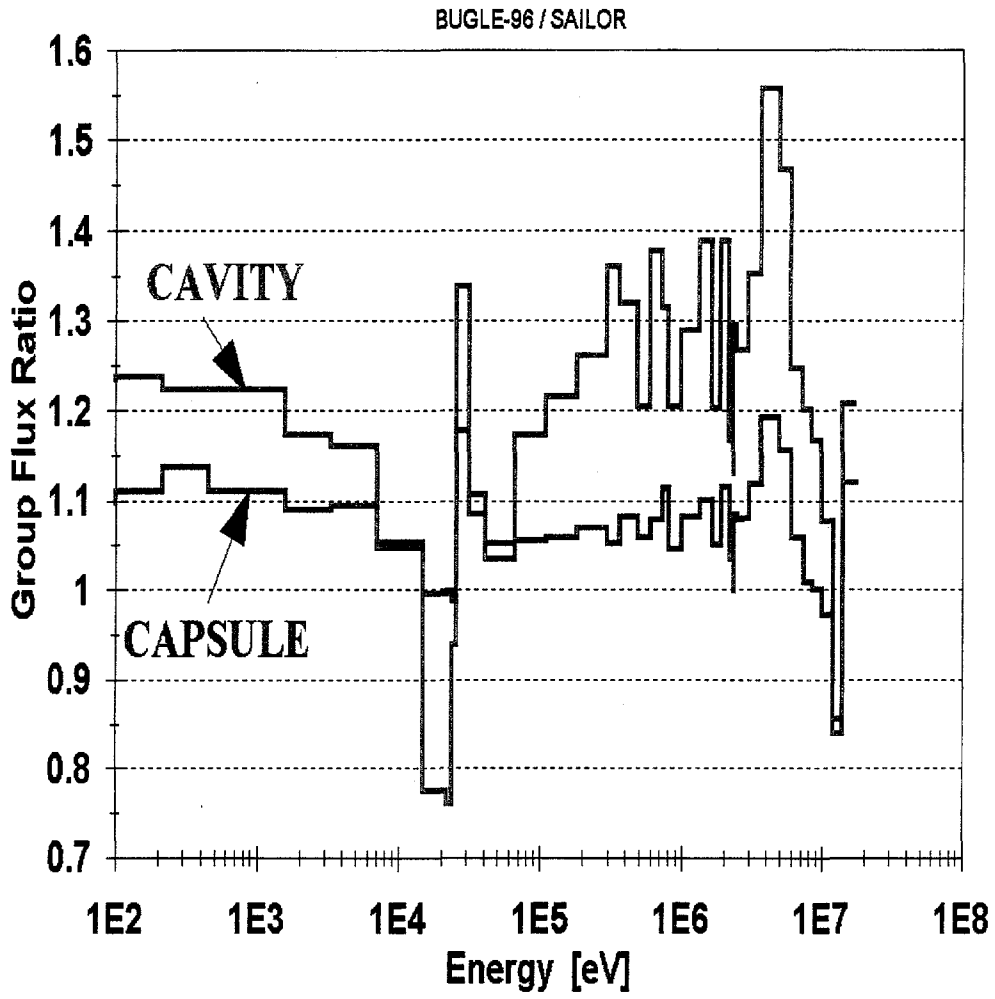

Figure 1 **The ratios of the group fluxes, calculated with the BUGLE-96 and SAILOR libraries, in the surveillance capsule and at the location of dosimeters in the cavity. ENDF/B-VI fission spectra were used with both BUGLE-96 and SAILOR libraries.**

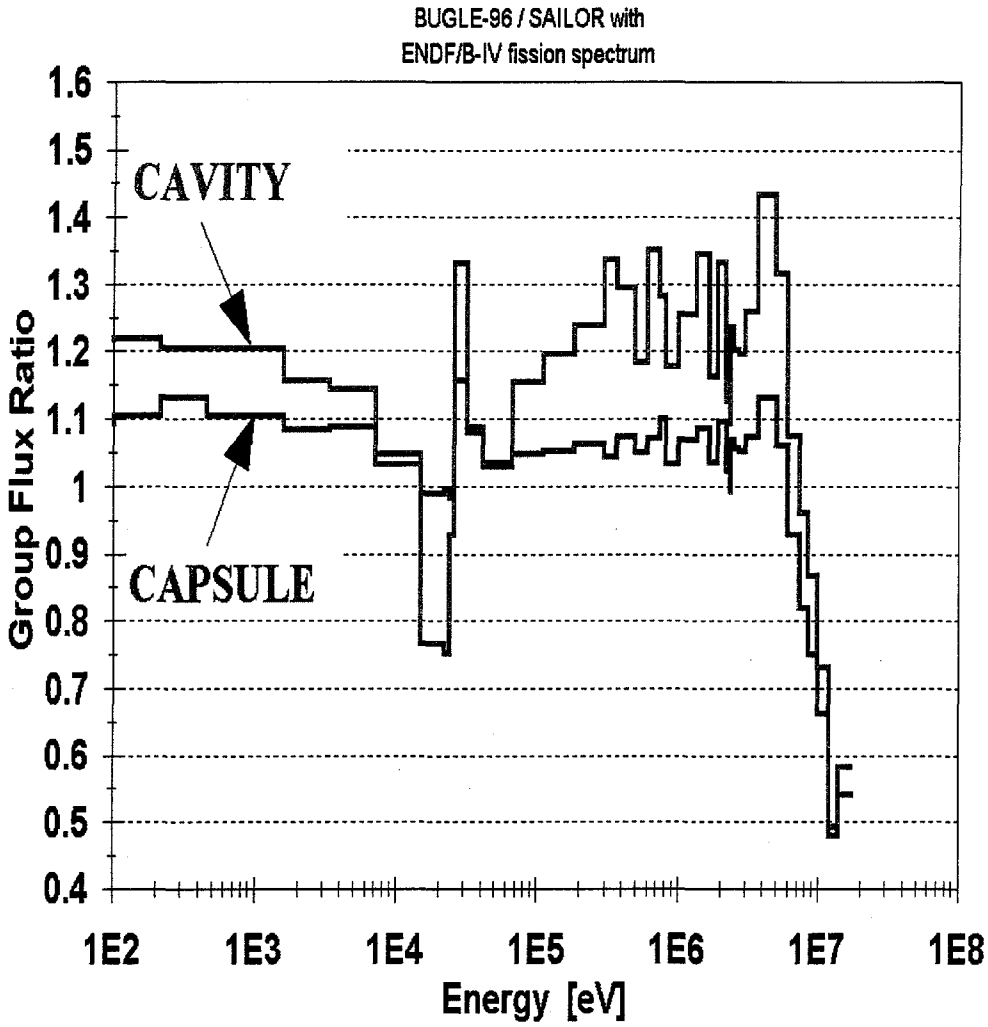

Figure 2 **The ratios of the group fluxes, calculated with the BUGLE-96 and SAILOR libraries, in the surveillance capsule and at the location of dosimeters in the cavity. The calculations with the SAILOR library utilized ENDF/B-IV fission spectra**

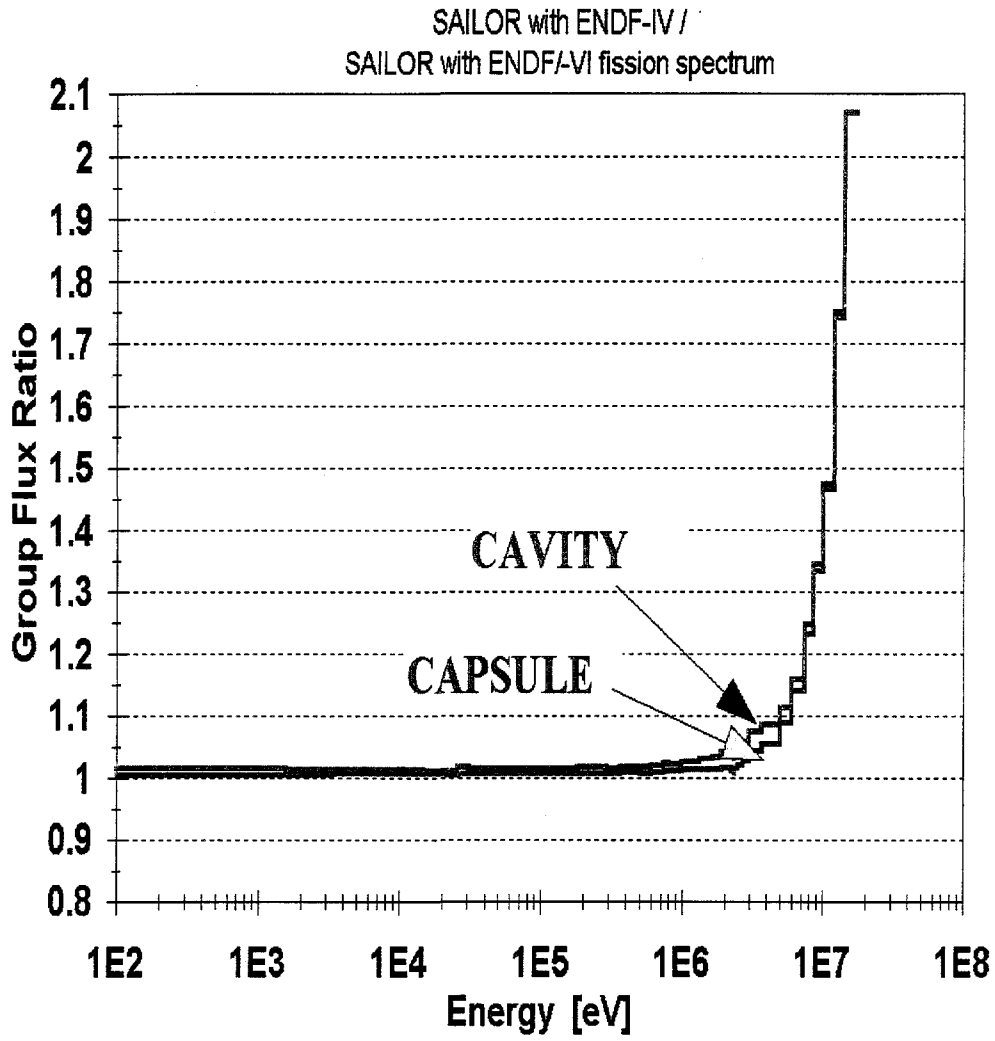

Figure 3 **The ratios of group fluxes, calculated with the SAILOR library and the ENDF/B-IV and ENDF/B-VI fission spectra, in the surveillance capsule and at the location of dosimeters in the cavity**

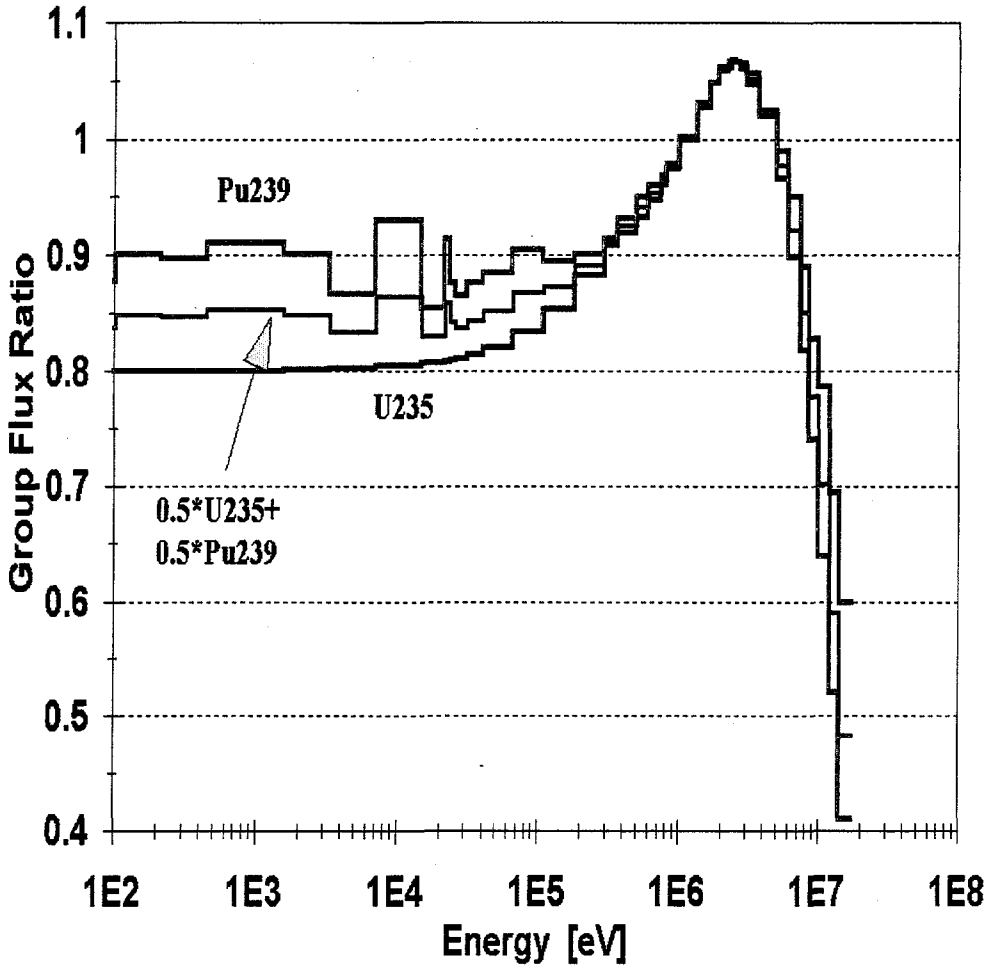

Figure 4 The ratios of fission spectra (BUGLE-96/SAILOR) for the ^{235}U, ^{239}Pu, and the average of the ^{235}U and ^{239}Pu spectra, from the BUGLE-96 and SAILOR libraries

INTERNAL DISTRIBUTION

1. K. J. Clayton
2. H. T. Hunter
3. D. T. Ingersoll
4. M. A. Kuliasha
5. J. V. Pace III
6. C. E. Pugh
7. I. Remec
8. C. H. Shappert
9. D. B. Simpson
10. J. A. Wang
11. R. M. Westfall
12. J. E. White
13. B. A. Worley
14. Central Research Library
15-16. Laboratory Records for Submission to OSTI
17. Laboratory Records - RC

EXTERNAL DISTRIBUTION

18. A. Abderrahim, SCK/CEN Fuel Research Unit, Boeretang 200, B-2400 MOL, Belgium
19. J. Adams, NIST, Bldg. 235, A-156, Gaithersburg, MD 20899-0001
20. A. F. Albornoz, National Atomic Energy Comm., Advanced Reactors Phys. Div., Ar. Ezequiel Bustillo 9500, 8400 San Carlos De Bariloche, Ris Negro, Argentine
21. S. L. Anderson, Radiation and Environmental Systems, Westinghouse Electric Corporation, Nuclear Energy Systems, Monroeville Nuclear Center, P.O. Box 355, Pittsburgh, PA 15230
22. J. F. Carew, Bldg. 130, Department of Nuclear Engineering, Brookhaven National Laboratory, Upton Long Island, New York 11973
23. J. W. Craig, U.S. Nuclear Regulatory Commission, Division of Engineering Technology, MS-T10D20, Washington, DC 20555-0001
24. I. Curl, AEA Technology plc, Reactor Physics, Shielding & Criticality Dept., Winfrith, Dorchester, Dorset, DT28DH, United Kingdom
25. P. D'Hondt, SCK/CEN, Boeretang 200, B-2400 MOL, Belgium
26. C. J. Fairbanks, U.S. Nuclear Regulatory Commission, Materials Engineering Branch, Two White Flint North, MS-T10E10, 11545 Rockville Pike, N. Bethesda, MD 20852-2783
27. P. J. Griffin, Radiation Metrology Laboratory, MS 1172, Sandia National Laboratories, P.O. Box 5800, Albuquerque, NM 87112
28. E. M. Hackett, U.S. Nuclear Regulatory Commission, Materials Engineering Branch, MS-T 10 E10, Washington, DC 20555
29. A. Haghighat, The Pennsylvania State University, 231 Sackett Bldg., University Park, PA 16802-1408
30. W. R. Jones, U.S. Nuclear Regulatory Commission, Reactor Analysis Branch, MS-T 4 A9, Washington, DC 20555
31. E. P. Lippincott, 1776 McClure Rd., Monroeville, PA 15146

32. L. Lois, Office of Nuclear Regulatory Research, Division of Systems Safety and Analysis, MS-ONFN8E23, Washington, DC 20555-0001
33. M. E. Mayfield, U.S. Nuclear Regulatory Commission, Materials Engineering Branch, MS-T10E10, N. Bethesda, MD 20852-2783
34. M. A. Mitchell, U.S. Nuclear Regulatory Commission, Materials and Chemical Engineering Branch, MS-O 7 D4, Washington, DC 20555
35. B. C. Na, OECD Nuclear Energy Agency, Le Seine St-Germain, 12 boul.des Iles, 92130 Issy les Moulineaux, France
36. E. Polke, Siemens-KWU, Freyeslebenstr.1, D-91058 Erlangen, Germany
37. G. Reffo, Italian National Agency for New Technology, C.R.E. e. CLEMENTEL, Via Martiri di Monte Sole n.4, 40129 - Bologna Italy
38. M. Suzuki, Reactor Component Reliability, Dept. Of Reactor Safety Res., JAERI, Tokai-mura, Ibaraki 319-11
39. R. D. Thompson, U.S. Nuclear Regulatory Commission, Property and Oversight Branch, Mail Stop T-7 I2, Washington, DC 20555-0001
40. W. T. Urban, Los Alamos National Laboratory, MS B 226 Los Alamos, New Mexico
41. J. G. Williams, University of Arizona, Nuclear Reactor Laboratory, Dept. of Nuclear & Energy Engineering, Tucson, AZ 85721
42. M. L. Williams, LSU Nuclear Science Center, Louisiana State University, Baton Rouge, LA 70803
43. S. Zaritsky, Kurchatov Institute, Kurchatov Square, 123182 Moscow, Russia